Journal Name

ARTICLE TYPE

Cite this: DOI: 10.1039/xxxxxxxxxx

Structure and Bonding in Crystalline Cesium Uranyl Tetrachloride under Pressure

Hussien H. Osman,[a,b] Pilar Pertierra,[a] Miguel A. Salvadó,[a,*] F. Izquierdo-Ruiz,[a] and J. M. Recio[a]

Received Date
Accepted Date

DOI: 10.1039/xxxxxxxxxx

www.rsc.org/journalname

A thorough investigation of pressure effects on the structural properties of crystalline cesium uranyl chloride was performed by means of first-principles calculations within the density functional theory framework. Total energies, equilibrium geometries and vibrational frequencies were computed at selected pressures up to 50 GPa. Zero pressure results present good agreement with available experimental and theoretical data. Our calculated equation of state parameters reveal that $Cs_2UO_2Cl_4$ is a high compressible material, similar to other ionic compounds with cesium cations, and displays a structural anisotropic behavior guided by the uranyl moiety. An unexpected variation of the U-O bond length, d_{UO}, is detected as pressure is applied. It leads to a d_{UO}-stretching frequency relationship that cannot be described by the traditional Badger's rule. Interestingly enough, it can be explained in terms of a change in the main factor controlling d_{UO}. At low pressure, the charge transferred to the uranyl cation induces an increasing of the bond length and a red shift of the stretching frequencies, whereas it is the mechanical effect of the applied pressure above 10 GPa the dominant factor that leads to a shortening of d_{UO} and a blue shift of the stretching frequencies.

Besides the interest of uranium-based compounds in the treatment of nuclear waste or as effective fuel materials especially for the light water reactors, uranyl complexes attracts experimental and theoretical attention due to the decisive role they play in the migration mechanisms of this radioactive element through the groundwater and soil.[1] In the last years, uranyl chloro complexes have been particularly studied using quantum-mechanical simulations and diverse spectroscopic techniques.[1–8] The nature of the chemical bonding in $Cs_2UO_2Cl_4$ was deeply studied by Zhurov *et al.*[3,4] using experimental X-ray diffraction electron densities. Vallet *et al.*[5] carried out a rigorous analysis of quantum mechanical calculations of uranyl complexes in gas phase and in a water solvent with different Lewis base ligands, providing interesting correlations between stretching frequencies, uranyl charges, and U-O bond lengths. X-ray diffraction and infrared and Raman spectroscopies have also been used to investigate how stretching frequencies correlate with U-O bond lengths in a variety of uranyl chloro complexes with emphasis in the evaluation of force (k_1) and interaction (k_{12}) constants involved in the UO_2 moiety.[5–7,9] In the experimental work of Schnaars and Wilson,[6,7] it was observed that Badger's rule[10] fails in actinyl complexes since a shorter distance is not always accompanied by a higher stretching force constant. Failure of Badger's rule was firstly detected by Vallet *et al.* in uranyl complexes with hydroxide ligands.[5] It is to be concluded that 'a great deal of caution must be afforded ... when making inferences in regard to bond distances and bond strengths' from vibrational frequencies of uranyl-based compounds.[6,7]

Pressure is an interesting thermodynamic variable if we look for structure-property correlations (see for example Ref. 11). By applying pressure, we can significantly modify the interatomic distances and the local environment of the uranyl moiety in $Cs_2UO_2Cl_4$, in a similar way as in previous studies with different ligands and countercations.[2,5–8,12] In spite of the strong nature of the U-O multiple bond, small but meaningful variations of its bond length could be observed under the pressure conditions attained in diamond anvil cell experiments. Quantum-mechanical simulations constitute an attractive alternative to recreate these conditions and provide valuable information on how structural changes affect force constants, charge transfer, and stretching frequencies of the uranyl moiety. However, in the case of solid $Cs_2UO_2Cl_4$, we are not aware of any previous theoretical or experimental investigation on its behavior under hydrostatic pressure.

In this study, we seek to fulfill a two-fold objective. Firstly,

[a] *MALTA-Consolider Team and Departamento de Química Física y Analítica, Universidad de Oviedo, E-33006, Oviedo, Spain.*
[b] *Department of Chemistry, Faculty of Science, Helwan University, Ain-Helwan, 11795, Cairo, Egypt.*
[*] *Corresponding author. E-mail: mass@uniovi.es*
Electronic supplementary information (ESI) available.

we pretend to provide detailed information on the response of the monoclinic structure of cesium uranyl chloride to hydrostatic pressure conditions up to 50 GPa. We believe that these novel results can arouse enough interest since they contribute to broad the fundamental knowledge of UO_2-based compounds. Secondly, a microscopic interpretation of the evolution with pressure of the U – O stretching modes is carried out to unveil relationships between the corresponding frequencies and force constants, atomic charges and bond distances associated with the uranyl cation. Our analysis also predict that Badger's rule is invalid in its traditional form, thus supporting the conclusions of Valet *et al.* [5] and Schnaars and Wilson. [6,7]

As regards our first aim, periodic first-principles electronic structure calculations were performed to optimize all the structural degrees of freedom of the monoclinic unit cell of $Cs_2UO_2Cl_4$ at selected pressures in the 0-50 GPa range. We have a long-term experience in quantum-mechanical simulations of the behavior of materials under high-pressure conditions, from the determination of isothermal equations of state in simple binary compounds [13,14] to the detailed description of phase transition mechanisms [15] and the structural prediction of novel materials. [16] We know that, although conventional density functional theory (DFT) under the local density approximation (LDA) or the generalized gradient approximation (GGA) usually gives a good agreement between theory and experimental data, these levels of calculation usually fail to capture the strong on-site Coulomb repulsion of the 5*f* electrons, and consequently predict incorrect ground states. One promising way to improve LDA and GGA approaches is by using the Hubbard parameter (U) through the so-called LDA/GGA+U approaches. [17,18] Therefore, we have examined different DFT+U levels of calculation following previous analysis in solid UO_2, [19,20] with explicit comparisons with available experimental and theoretical data. [3,21]

Concerning our second aim, two main factors were analyzed to rationalize the values of the symmetric stretching frequency of the uranyl moiety: charge and U – O bond length. In our previous work on the vibrational modes in uranyl aquo complexes, we have seen that all the frequencies, except the stretching modes associated with the U – O bond, have values below 400 cm^{-1}. [8] It has been repeatedly reported that depending on the medium and equatorial ligand type, the frequencies of the stretching modes can oscillate between 800-900 cm^{-1}. [5–8,12] As our interest is in the U-O chemical bond, we will focus on the variation of the stretching frequencies with respect to pressure, and how force constants, Bader charges, and bond lengths correlate with the observed trend.

The rest of the paper is divided into three more sections. In the next one, we describe in detail the monoclinic structure of $Cs_2UO_2Cl_4$ and collect the computational details of our calculations. Section III contains the results and discussion and is divided into two main subsections. The first one deals with pressure effects on the unit cell and the equation of state (EOS) parameters. The second one presents our analysis on the correlations between bond lengths, stretching frequencies and charge transfer involved in the uranyl moiety. The paper ends gathering the main conclusions of our work.

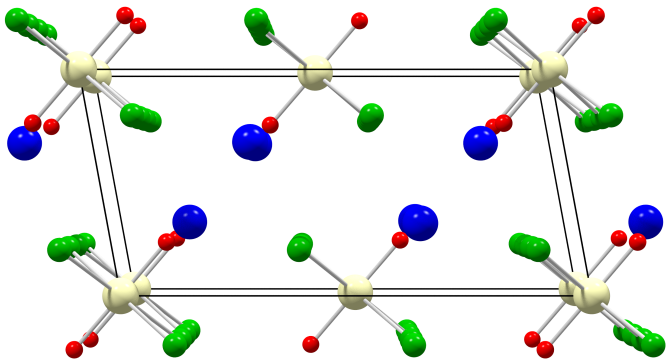

Fig. 1 *b*-axis projection of the unit cell of $Cs_2UO_2Cl_4$ (U = yellow, O = red, Cl = green, Cs = blue).

1 Structural and Computational Details

1.1 Crystal Description

The experimental crystal structure for $Cs_2UO_2Cl_4$ crystal has been previously reported. [3,4,21] $Cs_2UO_2Cl_4$ has a monoclinic structure, space group $C2/m$, with $Z = 2$. There are four independent atoms, one of each type, with seven free coordinates and four parameters defining the volume and shape of the crystal for a total of eleven degrees of freedom. The structure can be described as formed by $[UO_2Cl_4]^{2-}$ complex anions and Cs^+ cations. The complex anion consists of six ligands bound to the metal center in a pseudo-octahedral geometry. The axial positions are occupied by the two oxo ligands, while the four chloride ligands reside in the equatorial plane (see Figure 1 and Figure 2). The complex anion has a D_{4h} symmetry when in aqueous solution, in the crystal the uranium atom resides on a special position with C_{2h} site symmetry, C_2 axis goes along b direction and σ_h plane is parallel to the ac plane, resulting in a strictly linear conformation of the uranyl moiety and the four chlorine atoms located in the same plane. Deviations from the higher symmetry are small. The experimental angle between chlorine plane and uranyl is 89.4° and between Cl-U bonds is 87.2°. All the U-O bonds are parallel to each other, perpendicular to b axis and point approximately in the [201] direction forming an angle of 49.5° with the a axis that is very close to a half the β monoclinic angle.

The crystal packing can be described as a very distorted hexagonal close-packed structure where one third of sites are occupied by the complex anion and two thirds are occupied by cesium cations. In Figure 1 can be seen the stacking of successive layers of anions and cations parallel to the (110) plane. Also, hexagonal layers of mixed anions and cations are formed parallel to the $(\bar{2}01)$ plane. These layers contain also the uranyl bond. Each anion is surrounded by six cations in the plane and six additional ones in contiguous layers leading to a total twelve coordination.

1.2 Computational Methods

Electronic structure calculations were performed using the projector-augmented wave (PAW) and plane waves basis set scheme implemented in the Vienna *ab initio* simulation package (VASP). [22–24] Our computational strategy started with a thorough

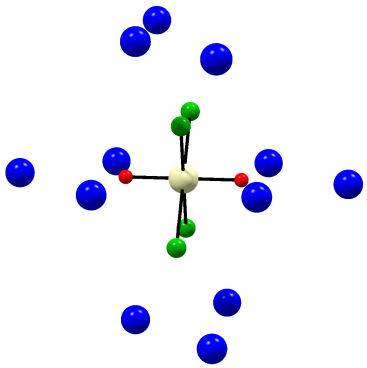

Fig. 2 Complex anion environment in $Cs_2UO_2Cl_4$.

computational study aimed to explore how the density functional (DFT) framework performs under LDA, GGA and LDA/GGA+U approximations.[25] The on-site Coulomb repulsion among the localized 5f electrons is described with the formalism of Dudarev *et al.*[26] In this scheme, the spherically averaged screened Coulomb energy (U) and the exchange energy (J) do not enter separately, only the difference ($U-J$) is meaningful and important for the total LDA/GGA energy functional, that is called the effective Hubbard term U_{eff}. After careful comparisons with experimental data (see below), we choose U_{eff} = 3.49 eV, which is lower than values used in previous works on UO_2.[27–29] Brillouin-zone integrals were approximated using Γ-centered Monkhorst-Pack meshes[30] where the numbers of subdivisions along each reciprocal lattice vector $\vec{b}_i$ were given by $N_i = \max(1, 15 \times |\vec{b}_i| + 0.5)$. The wavefunction was expanded in plane waves up to a cut-off energy of 520 eV to ensure convergence of the total energy within 10^{-3} eV/atom.

Lattice parameters and atomic positions were optimized at selected volumes and calculations were stopped when the forces on atoms were lower than 10^{-5} eV/Å. The equilibrium volume, bulk modulus (B_0) and its pressure derivative (B_0'), both evaluated at zero pressure, were obtained by fitting the 4^{th} order static Birch–Murnaghan equation of state to the calculated energy-volume data set using GIBBS code.[31] For all the optimized structures, topological analysis of the electron density were carried out using the Bader partitioning method[32] under the Henkelman group code[33] to compute atomic volumes and charges. Bond critical points and electron density at critical points were obtained using the program CRITIC2[34]. Frequencies were also calculated using the finite displacement method with a step of 0.008 Å and four displacements at all the optimized equilibrium geometries. Crystal structures were visualized using VESTA[35].

2 Results and Discussion

2.1 Crystal structure and equation of state

The equilibrium volume, lattice parameters (a, b, c, β) and selected bond lengths and angles obtained with several approximations at zero pressure are summarized in Table 1. When compared with the experimental values[4] of a, b, c and the monoclinic angle β, (11.788, 7.641, 5.769 Å, and 100.44°, respectively), our GGA (PBEsol) + U results show a very good agreement. It is also

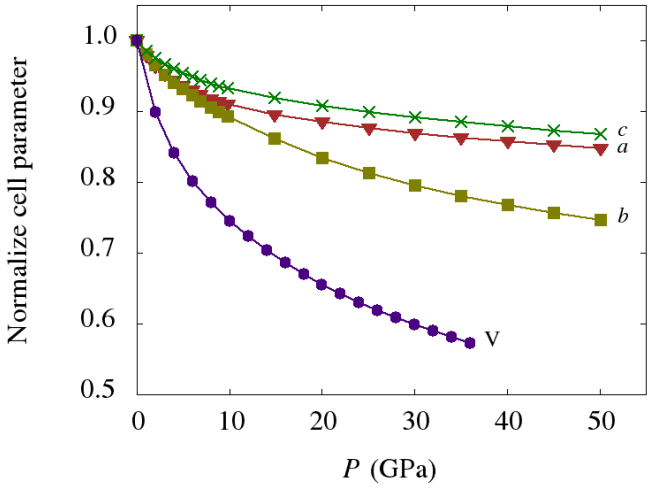

Fig. 3 Normalized cell parameters and unit cell volume of $Cs_2UO_2Cl_4$ with respect to hydrostatic pressure according to our calculations. Symbols stand for a (triangle), b (square), c (cross), and V (circle).

the best level of calculation if we look at the U-O bond length (d_{UO}=1.775 Å calculated and 1.774 Å experimental value from Zhurov *et al.*[4]), which is a key parameter in our discussion of the next section. Other interatomic distances and angles agrees very well with the corresponding experimental data, thus keeping the whole point group symmetry around the uranyl moiety. Although other levels of calculation also show a consistent description of the $Cs_2UO_2Cl_4$ structure, in the rest of this paper our results will refer only to this PBEsol+U level of calculation.

The overall effect of pressure on the volume and unit cell parameters can be seen in Figure 3. The unit cell volume of $Cs_2UO_2Cl_4$ exhibits a high compressible trend with a reduction of about 50 % in the 0-50 GPa range. EOS parameters, B_0=16.5 GPa and B_0'=4.9, characterize a molecular-ionic class of compound with a high incompressible UO_2 dication in a quite open structure with empty space (low electron density) among cations and anions. It is noticeable that our calculated B_0 value lies in the range of other binary cesium halides. For example, the zero pressure bulk modulus in CsCl is 16.7 GPa.[36]

Lattice parameters a and c decrease by about 15 % in the 0-50 GPa pressure range, while b changes to a greater extent, by about 25 % of reduction, the zero pressure value. Thus, the easy axis to compress in $Cs_2UO_2Cl_4$ is the b-axis, which is perpendicular to the uranyl bond. Also, we obtained an increase in the value of the monoclinic angle (β) of 8 %, that can be ultimately related with the orientation of the uranyl moiety in the unit cell. Overall, the calculated response of $Cs_2UO_2Cl_4$ under hydrostatic pressure shows that the structural anisotropy of this material is quite significant.

2.2 Pressure effects on local environments, stretching frequencies, and topological charges

Pressure affects the local geometry by changing interatomic distances and bond angles. The main bond lengths, d_{UO}, d_{UCl}, and

Table 1 Comparison between zero pressure calculated and experimental data (Reference 4) of lattice parameters (Å), volume (Å^3), shortest bond U-O (d_{UO}), U-Cl (d_{UCl}), and Cs-O (d_{CsO}) distances (Å) and Cl-U-O (ω_1) and Cl-U-Cl (ω_2) bond angles (°).

	a	b	c	β	V	d_{UO}	d_{UCl}	d_{CsO}	ω_1	ω_2
LDA	11.56	7.33	5.70	102.0	472.4	1.803	2.618	3.02	90.6	92.4
LDA+U	11.52	7.47	5.66	101.5	476.8	1.770	2.653	3.09	90.6	93.0
PBE	12.26	7.84	5.98	100.9	565.0	1.815	2.678	3.35	90.8	93.1
PBE+U	12.36	7.89	5.95	96.8	576.5	1.780	2.717	3.74	90.9	92.9
PBEsol	11.88	7.57	5.83	101.5	513.7	1.808	2.641	3.18	90.7	92.9
PBEsol+U	11.88	7.68	5.79	100.0	520.8	1.775	2.678	3.32	90.7	93.3
Exp.	11.79	7.64	5.77	100.4	511.01	1.774	2.671	3.32	90.3	92.9

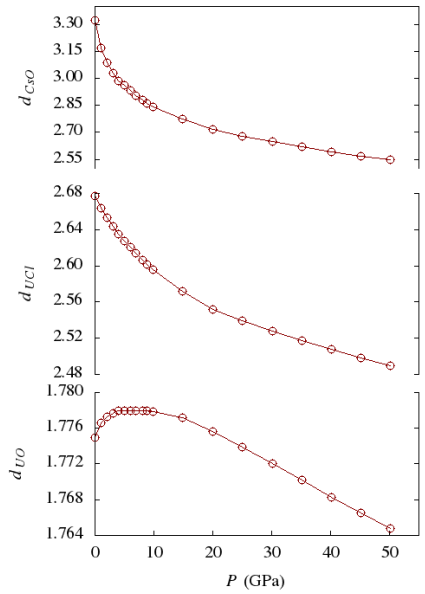

Fig. 4 Relevant bond lengths in $Cs_2UO_2Cl_4$ with respect to hydrostatic pressure according to our calculations. Distances in Å.

d_{CsO}, are examined in Fig. 4. As expected, globally the distances decrease as hydrostatic pressure is applied. In the whole 0-50 GPa pressure range, the U–O, U–Cl and Cs–O distances reduce by 0.010, 0.188 and 0.953 Å, respectively. d_{UO} variations induced by different environments in previous works are of the same order: 0.010 Å [6], 0.012 Å [7], 0.013 Å [12], 0.020 Å.[8] However, rather surprisingly, d_{UO} increases by 0.006 Å in the low pressure regime (up to approximately 10 GPa). An examination of the electron density at the bond critical points (bcp's) shows values of 0.063 for U–Cl, 0.316 for U–O and 0.0078 e/bohr^3 for O–Cs at zero pressure. These results are in accordance with experimental data[4] and cluster calculations.[5] When pressure increases both U–Cl and O–Cs electron densities at the bcp increase monotonously. However, in the case of U–O, the electron density at its bcp decreases to a minimum value of 0.312 e/bohr^3 at 10 GPa and then shows the increasing trend as pressure increases up to 50 GPa (see Fig. S1, ESI). Moreover, these results are consistent with the behavior displayed by our bond length data in Fig. 4. These facts are fully consistent with a weakening of the U–O bond manifested by frequency parameters in the low pressure regime, as we will see below. To explain this fact, we have to go further into the behavior of other distances and the effect of electrostatic interactions. We observe that 77 % of the total shortening of Cs–O bond length occurs in the 0–10 GPa region, where d_{CsO} decreases by 0.481 Å. Similar behavior is obtained for the U–Cl distance, about half the change takes place up to 10 GPa with a reduction of 0.082 Å. As discussed by Vallet *et al.*[5], a drop in the ligand-U distance correlates with a lengthening of the U-O distance due to the electrostatic repulsions between the yl-oxygens and the negatively charged chloride ligands. Moreover, as we will discuss in detail later, it should be also emphasized that as pressure is applied the charge transferred to the uranyl moiety increases. This effect tends to enlarge the U-O and can be only compensated at high enough pressures by the effect of other atoms approaching the oxygen atom. In order to test this hypothesis we have made electronic structure calculations in a model system comprising an *in vacuo* UO_2Cl_4 cluster with two Cs atoms located in the line O-U-O above and below the chlorines plane (see ESI for computational details). For a fixed U–Cs distance, decreasing U–Cl distance leads to longer U–O bond as expected (Fig. S3, ESI). For a fixed U–Cl distance, decreasing U–Cs distance also lead first to a longer U–O bond (electrostatic attractive effect) but at certain distance the behavior is reversed (Pauli repulsion). The obtained curve (Fig. S4, ESI) shows the same qualitative behavior as the one we can see in Fig. 4 for d_{UO} with respect to pressure in the crystal. This supports our hypothesis of competing factors determining the final U-O bond distance in the crystal.

The angle between the U–Cl and U–O bonds (ω_2 or ω_3) is negligibly affected by pressure, thus remaining close to 90° in the 0-50 GPa range. On the other hand, the two supplementary Cl–U–Cl angles in the equatorial plane (ω_1 and ω_4) change by about 21° over the whole pressure range as shown in Figure 5. It is energetically preferable to change the equatorial angle maintaining the uranyl bond perpendicular to it. When the pressure increases and the cell is compressed, the repulsion forces between chloride atoms can be minimized increasing one Cl–U–Cl angle and decreasing the other one making the b axis the preferred compression direction. It is remarkable that close to 10 GPa all ω_i-p curves cross with a value of 90°.

The local distortions induced by pressure lead to changes in the U-O bond strength that can be quantified evaluating parameters associated to the symmetric and antisymmetric stretching modes of the uranyl moiety. Typical values of ν_1 and ν_3 in the UO_2Cl_4

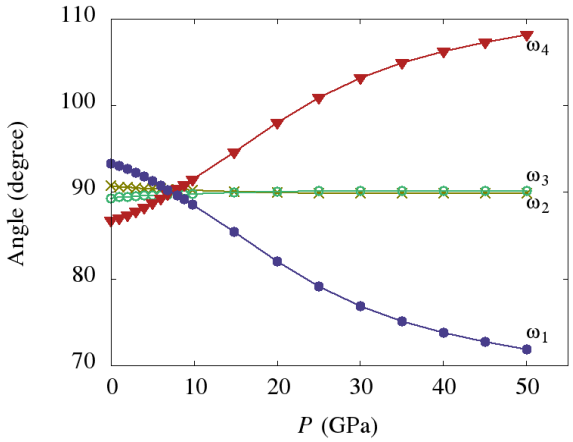

Fig. 5 Main bond angles of the UO_2Cl_4 complex anion in the $Cs_2UO_2Cl_4$ crystal with respect to hydrostatic pressure according to our calculations. See text for definition of ω_i symbols.

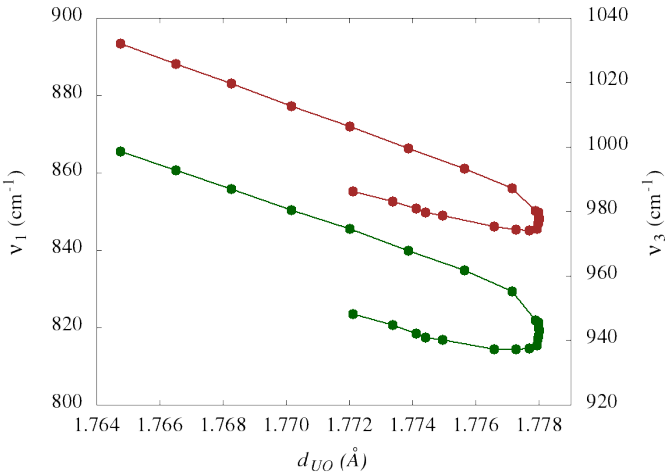

Fig. 6 Frequencies of the symmetric (lower curve, left axis) and antisymmetric (upper curve, right axis) stretching modes of uranyl with respect to d_{UO} bond length according to our calculations.

complex anion lie within the 831–842 cm^{-1} and 900–922 cm^{-1} ranges, respectively.[6,7] Our calculated crystalline vibrational frequencies of the symmetric and antisymmetric modes at zero pressure are 818 cm^{-1} (832 cm^{-1}) and 979 cm^{-1} (922 cm^{-1}). Deviations with respect to experimental values[6] (in brackets) are lower than 2 % and 7 %, respectively. Overall, the pressure evolution of these frequencies shows a typical slightly sublinear trend being the splitting between ν_1 and ν_3 almost constant along the pressure range of our study. When we plot the stretching frequencies against d_{UO} (see Fig. 6), we find a two branches-like behavior for both frequencies. In each branch the expected relationship between shorter bond and increased frequency is found. We notice that the jump from one branch to the other occurs at the d_{UO} value obtained around 8 GPa. This result is a manifestation of the d_{UO}-p behavior previously discussed (see Fig. 4, bottom).

We calculated the stretching force constant, k_1, and the interaction force constant, k_{12} from the computed frequencies[6] (see Fig. 7). k_1 is a measure of the strength of the U-O bond, whereas k_{12} describes the interaction between the two yl-oxygen atoms. The actual expressions relating k_1 and k_{12} with ν_1 and ν_3 can be found elsewhere (see for example equations (3) and (4) of Ref. 9 or the supplementary material of Ref. 6). Here, it is important to point out that besides the mass dependences, k_1 and k_{12} roughly depends, respectively, on the sum and difference of these frequencies. Our calculated values fall between 7.06 and 7.95 for k_1 and -0.804 and -0.900 for k_{12} in the 0–50 GPa range. The values of Schnaars and Wilson in a variety of UO_2-based compounds[6,7] span across 6.58 to 6.82 and -0.18 to -0.27 for k_1 and k_{12}, respectively. In plutonyl complex anions the interaction force constant shows values as low as -0.53.[6] With respect to our calculated values, the difference in k_{12} is easily explained in terms of the higher ν_3 computed value and the sensitivity of the model to the input frequencies. Besides, it is to be pointed out that our negative k_{12} values are consistent with the inverse trans influence experienced by dioxo actinyl compounds that generates negative $\nu_1 - \nu_3$ differences. Although k_{12} has a relatively small change in the computed pressure range, it exhibits a maximum in a zone close to the jump in the frequencies branches discussed above.

A formal relationship between d_{UO} and k_1 can be described with the Badger's rule,[10] expressed here as $k_1^{-1/3} = A^{-1/3}(d_{UO} - B)$ (A and B are fitting parameters) which implicitly contains the more general rule that a shorter bond has a larger stretching force constant. Derived relationships were used by Bartlett and Cooney to predict U–O bond lengths from stretching frequencies with varying success.[9] We clearly observed that our data cannot be described by a unique Badger's relationship (see top and bottom straight lines in Fig. 7 right). Interestingly enough, we see, however, that these two Badger linear trends describe accurately the correlation between d_{UO} and k_1. From our fittings we obtain 0.65 and 1.00 mdyn $Å^2$, to be compared with the universal Badger parameter $A = 1.86$ mdyn $Å^2$.[37,38] Thus, our data does corroborate previous results on studies of dioxo actinyl compounds regarding Badger's rule failure.[5–7]

Nevertheless, it is possible to explain this anomalous behavior of Badger's rule by means of a deeper analysis of the two main factors affecting frequencies and distances as pressure is applied. The first factor is the pure mechanical effect that produces an overall shortening of interatomic distances in the crystal. The second one acts in the opposite direction as far as the d_{UO} distance is concerned. It is the charge transferred to the UO_2 moiety. The idea is to separate both factors and evaluate the fulfillment of Badger's rule without considering charge transfer effects. Before this analysis is introduced, we recall to previous results on the charge transfer in uranyl hydrated species[12] along with our own results at this regard.

As formerly illustrated by Siboulet *et al.*,[12] the charge transferred to the uranyl dication is a good parameter to explain changes in the U-O bond length and stretching frequencies involved in the uranyl moiety. At zero pressure, our topological analysis of the electron density leads to a total charge of the $Cs_2UO_2Cl_4$ unit cell of 0.0001 e, and a unit cell volume calculated from separate atomic volumes of 520.75 $Å^3$. These values are consistent with the neutral character of the cell and with the

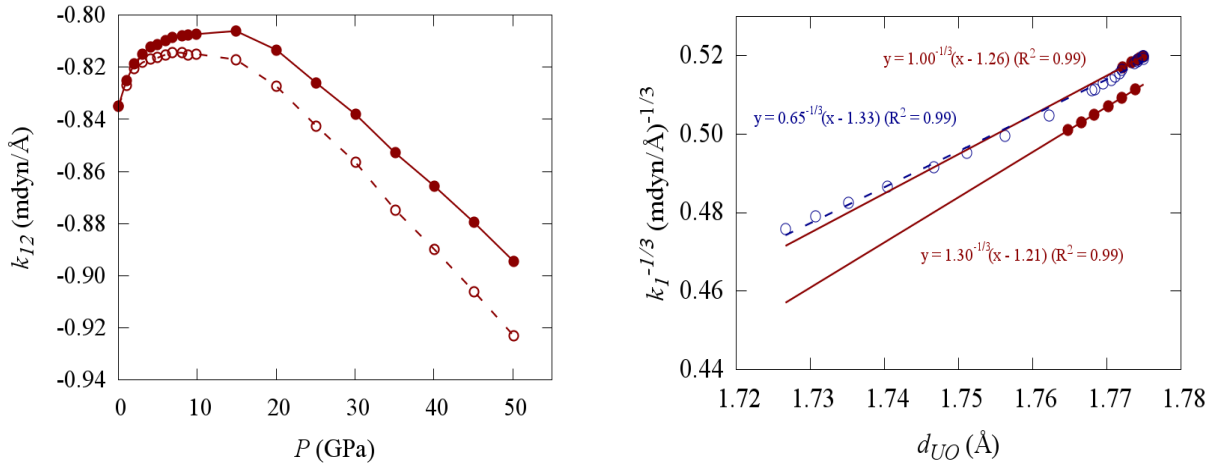

Fig. 7 Interaction O_{yl}-O_{yl} constant with respect to hydrostatic pressure (left) and force constant-bond length linear correlations in the U-O chemical bond (right) according to our calculations. Results from the pure mechanical model are displayed (dashed lines and empty circles).

Table 2 Atomic charges (q, e) and atomic volumes (Ω, Å^3) for $Cs_2UO_2Cl_4$ crystal.

	U	O	Cl	Cs	UO_2	
q	2.756	-0.878	-0.685	0.871	1.000	Present
	2.751	-0.923	-0.605	0.774	0.905	Exp. 4
Ω	17.04	19.13	32.64	37.26	55.30	Present
	16.17	18.99	31.39	37.73	54.15	Exp. 4

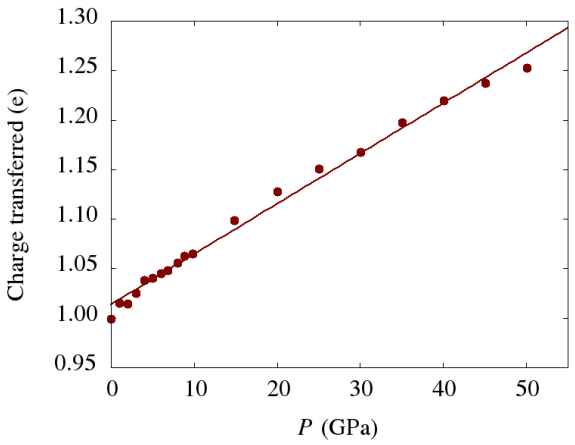

Fig. 8 Bader charge transferred versus pressure. R^2 = 0.996 and the slope corresponds to 0.005 GPa per electron transferred.

optimized cell volume. Our calculated charges and volumes are close to those obtained from the topological analysis carried out by Zhurov *et al.* using experimental charge densities of the same crystal at 20 K (see Table 2). This experimental study gives a total charge of uranyl of +0.905 e, while we obtain a value of 1.00 e. For this moiety we previously obtained a value of 0.996 e for the same complex in water solution.[8]

The effect of pressure on the charge transferred to uranyl, calculated as the difference between the uranyl formal charge (+2) and the calculated one, is presented in Figure 8. The uranyl charge decreases as the pressure increases. The charge transferred to uranyl increases by 25 % of its zero pressure value when pressure increases up to 50 GPa.

Let us propose now an analysis of Badger's rule using k_1-d_{UO} data coming from results involving only the pure mechanical effects on frequencies and distances. A simple yet reasonable procedure consists in removing the reduction in frequencies and the increasing in distances induced by the charge transferred to the uranyl moiety. At a given pressure, $\nu_1(p)$ and $d_{UO}(p)$ can be described with these expressions:

$$\nu_s(p) = \nu_1(0) + \Delta\nu_1(p); \quad \Delta\nu_1(p) = \Delta\nu_1^M(p) + \Delta\nu_1^{CT}(p)$$

$$d_{UO}(p) = d_{UO}(0) + \Delta d_{UO}(p); \quad \Delta d_{UO}(p) = \Delta d_{UO}^M(p) + \Delta d_{UO}^{CT}(p) \quad (1)$$

where the superscripts M and CT stand, respectively, for the contributions due to pure mechanical and charge transfer effects. We can use the proposed slopes reported by Siboulet *et al.*[12] for the charge transfer effect in the frequency, -300 cm^{-1}, and the distance, +0.16 Å, both per electron transferred to the uranyl moiety. Taking the charge transferred at zero pressure as the reference value, we can obtain the contributions to the frequencies and distances at different pressures using the above slopes and the calculated relationship between pressure and charge transferred displayed in Figure 8. With this information we can evaluate new frequencies and distances only affected by the pure mechanical effect using the following expressions:

$$\nu_1^M(p) = \nu_1(0) + \Delta\nu_1^M(p); \quad d_{UO}^M(p) = d_{UO}(0) + \Delta d_{UO}^M(p) \quad (2)$$

Similar equations can be written for ν_3 providing the basic data, along with d_{UO}^M values, for a new analysis of Badger's rule. Results are included in Fig. 7, and illustrate how the fulfillment of this rule is achieved. Successfully, a single straight line can now describe the correlation between the force constant and the bond length (see Fig. 7 right). From this fittings we obtain for the Badger parameter A = 1.30 mdyn Å^2.

We also considered the behavior of uranyl charge and the symmetric stretching Raman frequency versus the U–O distance as

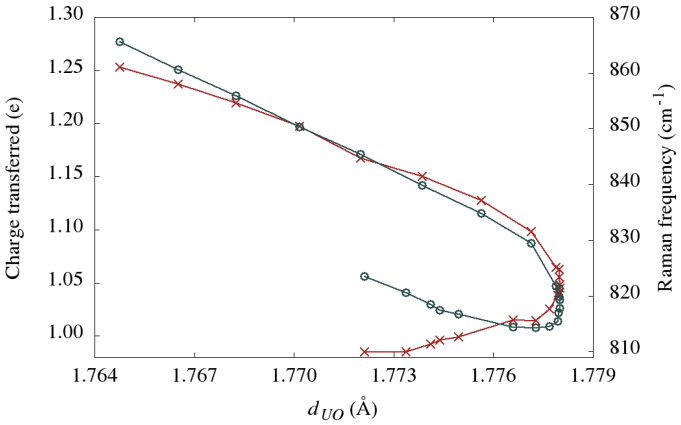

Fig. 9 Bader charge transferred (cross, left axis) and Raman frequency (circle, right axis) versus uranyl bond length.

shown in Figure 9. The ν_s–d_{UO} shows three different regimes: (i) ν_s decreases around 4 cm^{-1} at low pressures up to 5 GPa, (ii) from 5 to 10 GPa the blue shift is around 8 cm^{-1}, and (iii) an increase around 40 cm^{-1} is observed in the high pressure range from 10 to 50 GPa. Both, at low and high pressure ranges the shorter the bond length the larger the Raman frequency but around 8 GPa, when d_{UO}=1.778 Å, the blue shift of around 8 cm^{-1} in ν_s appears without bond length variation. A linear correlation between the U–O distance and the Raman-active vibrational frequency with a slope of 20 cm^{-1}/pm was proposed by Siboulet *et al.* [12] when different aquo uranyl complexes were considered. A similar behavior can be derived from our calculations in crystalline $Cs_2UO_2Cl_4$ but in two different pressure regions. In the low pressure regime the decrease in the Raman frequency (and the accompanied increase in bond length) is associated with a decrease in the uranyl charge, that is the same behavior found by Siboulet *et al.* Our $\Delta\nu_s/\Delta d_{UO}$ ratio is only around 10 cm^{-1}. The lower slope can be attributed to a greater Δd_{UO} value than expected from the charge transferred to the uranyl dication. This effect is caused by an enhancement of attractive electrostatic interactions of the Cs cations that display a very rapid reduction of their distances to the yl-oxygen atoms in the low pressure regime, as we have seen in Fig. 4. However, at pressures higher than 10 GPa the charge transfer is not a good parameter to correlate with distances and symmetric stretching frequencies: an increase in the Raman frequency (and the accompanying bond length decrease) occur in spite of the increase of the charge transferred to UO_2. This is due to a pure mechanical effect of hydrostatic pressure that reduces the d_{UO} distance, strengthening the U-O bond, and leads to a blue shift in the stretching frequencies. What is more, d_{CsO} distances enter in the repulsive regime and this interaction starts pushing rather than pulling the U-O bond.

3 Conclusions

The exam of the behavior of $Cs_2UO_2Cl_4$ under hydrostatic pressure reveals that this compound is quite compressible and exhibits a structural anisotropy mainly controlled by the orientation of the uranyl moiety. d_{UO}, d_{UCl}, and d_{CsO} distances decrease roughly 0.01 Å, 0.20 Å, and 0.95 Å in the 0-50 GPa pressure range, thus providing information on the strengths of bonds and interaction, and also on the main mechanisms of volume reduction under applied pressure. Our calculated equation of state parameters are new to the best of our knowledge, and deserve experimental measurements to be contrasted with.

In addition to structural data, vibrational stretching frequencies were calculated in order to analyze their correlation with U–O bond lengths and the charge transferred to UO_2. According to our calculations, d_{UO} shows two opposite trends under hydrostatic pressure: an unexpected increasing of 0.006 Å in the low pressure regime is followed by a quasi-linear decreasing trend up to 50 GPa. We obtain different force constants for uranyl bonds of same length that causes Badger's rule to be invalid in its traditional form. We found a plausible interpretation in terms of the main factor controlling d_{UO}-stretching frequency relationships. The charge transferred to uranyl is a key factor in the low pressure region resulting in a red shift trend for the Raman symmetric stretching frequency. Pressure-induced shortening of distances dominates the ν_1–d_{UO} trend at pressures above 10 GPa. In this high pressure region, the mechanical effect leads to Cs–O interactions to enter in the repulsive region enhancing the shortening of the U–O distance, which results in a blue shift trend for the Raman frequency. Interestingly enough, in both regimes, independent Badger's linear relationships are found, though a unique correlation covering the whole pressure range can be also obtained when charge transfer effects are removed.

Acknowledgement

Financial support from MEDASTAR programme EMA–2 (2013/2015), the Spanish Ministerio de Economía y Competitividad (MINECO) under project CTQ2012-38599-C02-01 and Principado de Asturias under GRUPIN14-049 project are gratefully acknowledged.

References

1 M. Dargent, J. Dubessy, L. Truche, E. F. Bazarkina, C. Nguyen-Trung, P. Robert, *Eur. J. Mineral.*, 2013, **25**, 765–775.
2 M. Buhl, N. Sieffert, V. Golubnychiy, G. Wipff, *J. Phys. Chem. A*, 2008, **112**, 2428–2436.
3 V. V. Zhurov, E. A. Zhurova, A. A. Pinkerton, *Inorg. Chem.*, 2011, **50**, 6330–6333.
4 V. V. Zhurov, E. A. Zhurova, A. I. Stash, A. A. Pinkerton, *J. Phys. Chem. A*, 2011, **115**, 13016–13023.
5 V. Vallet, U. Wahlgren, I. Grenthe, *J. Phys. Chem. A*, 2012, **116**, 12373–12380.
6 D. D. Schnaars, R. E. Wilson, *Inorg. Chem.*, 2013, **52**, 14138–14147.
7 D. D. Schnaars, R. E. Wilson, *Inorg. Chem.*, 2014, **53**, 11036–11045.
8 F. Izquierdo-Ruiz, J. M. Menéndez, J. M. Recio, *Theor. Chem. Acc.*, 2015, 134:7.
9 J. R. Bartlett, R. P. Cooney, *J. Mol. Struct.*, 1989, **193**, 295–300.
10 R. M. Badger, *J. Chem. Phys.*, 1934, **2**, 128–131.

11 J. M. Recio, J. M. Menéndez. A. Otero-de-la-Roza, Eds.; *An Introduction to High-Pressure Science and Technology*; CRC Press: Boca Raton, 2015.

12 B. Siboulet, C. J. Marsden, P. Vitorge, *Chem. Phys.*, 2006, **326**, 289–296.

13 V. Luaña, J. M. Recio, L. Pueyo, *Phys. Rev. B*, 1990, **42**, 1791-1801.

14 J. M. Recio, A. Martín Pendás, E. Francisco, M. Flórez, V. Luaña, *Phys. Rev. B*, 1993, **48**, 5891–5901.

15 M. A. Salvadó, P. Pertierra, A. Morales-García, J. M. Menéndez, J. M. Recio, *J. Phys. Chem. C*, 2013, **117**, 8950–8958.

16 M. Marqués, A. Morales-García, J. M. Menéndez, V. G. Baonza. J. M. Recio, *Phys. Chem. Chem. Phys*, 2015 (in press DOI: 10.1039/C5CP03673A).

17 S. L. Dudarev, D. N. Manh, A. P. Sutton, *Philos. Mag. B*, 1997, **75**, 613–628.

18 Y. Yun, H. Kim, H. Lim, H.; K. Park, *J. Korean Phys. Soc.*, 2007, **50**, 1285–1289.

19 J. Wiktor, M. F. Barthe, G. Jomard, M. Torrent, M. Freyss, M. Bertolus, *Phys. Rev. B*, 2014, **90**, 184101/11.

20 B. Dorado, B. Amadon, M. Freyss, M. Bertolus, M *Phys. Rev. B*, 2009, **79**, 235125/8.

21 D. J. Watkin, R. G. Denning, K. Prout, *Acta Crystallogr. C*, 1991, **47**, 2517–2519.

22 P. E. Blöchl, *Phys. Rev. B*, 1994, **50**, 17953–17979.

23 G. Kresse, J. Furthmüller, *Phys. Rev. B*, 1996, **54**, 11169–11186.

24 G. Kresse, D. Joubert, *Phys. Rev. B*, 1999, **59**, 1758–1775.

25 J. P. Perdew, K. Burke, M. Ernzerhof, *Phys. Rev. Lett.*, 1996, **77**, 3865–3868.

26 S. L. Dudarev, G. A. Botton, S. Y. Savrasov, C. J. Humphreys, A. P. Sutton, *Phys. Rev. B*, 1998, **57**, 1505–1509.

27 H. Shi, M. Chu, P. Zhang, *J. Nucl. Mater.*, 2010, **400**, 151–156.

28 G. Kaur, P. Panigrahi, M. C. Valsakumar, *Modelling Simul. Mater. Sci. Eng.*, 2013, **21**, 065014.

29 J. Rabone, M. A. Krack, *Comput. Mater. Sci.*, 2013, **71**, 157–164.

30 H. J. Monkhorst, J. D. Pack, *Phys. Rev. B*, 1976, **13**, 5188–5192.

31 M. A. Blanco, E. Francisco, V. Luaña, *Comp. Phys. Comm.*, 2004, **158**, 57–72.

32 R. F. W. Bader, *Atoms in Molecules: A Quantum Theory*, The International Series of Monographs of Chemistry; Halpern, J., Green, M. L. H., Eds.; Clarendon Press: Oxford, U. K., 1990.

33 W. Tang, E. Sanville, G. Henkelman, *J. Phys.: Condens. Matter*, 2009, **21**, 084204/7.

34 A. Otero-de-la-Roza, E.R. Johnson and V. Luaña, *Comput. Phys. Commun.*, 2014, **185**, 1007.

35 K. Momma, F. Izumi, *J. Appl. Cryst.*, 2011, **44**, 1272–1276.

36 B. Xu, Q. Wang, Y. Tian, *Sci. Rep.*, 2013, **3**, 3068/7.

37 K. Nakamoto, *Infrared and Raman Spectra of Inorganic and Coordination Compounds Part A: Theory and Applications in Inorganic Chemistry*, 5th ed. ; John Wiley & Sons, Inc.: New York, 1997.

38 J. C. Weisshaar, *J. Chem. Phys.*, 1989, **90**, 1429–1433.